JOURNAL OF VIROLOGY, July 2002, p. 6689–6700 Vol. 76, No. 13
0022-538X/02/$04.00+0 DOI: 10.1128/JVI.76.13.6689–6700.2002

Human Immunodeficiency Virus Type 1 Enters Brain Microvascular Endothelia by Macropinocytosis Dependent on Lipid Rafts and the Mitogen-Activated Protein Kinase Signaling Pathway

Nancy Q. Liu,[1,2] Albert S. Lossinsky,[3] Waldemar Popik,[4] Xia Li,[1] Chandrasekhar Gujuluva,[1] Benjamin Kriederman,[5] Jaclyn Roberts,[1] Tatania Pushkarsky,[6] Michael Bukrinsky,[6] Marlys Witte,[5] Martin Weinand,[5] and Milan Fiala[1,2]*

Department of Medicine, Greater Los Angeles VA Medical Center, Los Angeles, California 90073[1]; Cardiovascular Research Laboratory, UCLA School of Medicine, Los Angeles, California 90095[2]; Neural Engineering Department, Huntington Medical Research Institutes, Pasadena, California 91105[3]; Oncology Center, The Johns Hopkins University School of Medicine, Baltimore, Maryland 21231[4]; Department of Surgery, University of Arizona, Tucson, Arizona 85724[5]; and Department of Microbiology and Tropical Medicine, The George Washington University, Washington, D.C. 20037[6]

Received 4 September 2001/Accepted 27 March 2002

Brain microvascular endothelial cells (BMVECs) present an incomplete barrier to human immunodeficiency virus type 1 (HIV-1) neuroinvasion. In order to clarify the mechanisms of HIV-1 invasion, we have examined HIV-1 uptake and transcellular penetration in an in vitro BMVEC model. No evidence of productive infection was observed by luciferase, PCR, and reverse transcriptase assays. Approximately 1% of viral RNA and 1% of infectious virus penetrated the BMVEC barrier without disruption of tight junctions. The virus upregulated ICAM-1 on plasma membranes and in cytoplasmic vesiculotubular structures. HIV-1 virions were entangled by microvilli and were taken into cytoplasmic vesicles through surface invaginations without fusion of the virus envelope with the plasma membrane. Subsequently, the cytoplasmic vesicles fused with lysosomes, the virions were lysed, and the vesicles diminished in size. Upon cell entry, HIV-1 colocalized with cholera toxin B, which targets lipid raft-associated GM1 ganglioside. Cholesterol-extracting agents, cyclodextrin and nystatin, and polyanion heparin significantly inhibited virus entry. Anti-CD4 had no effect and the chemokine AOP-RANTES had only a slight inhibitory effect on virus entry. HIV-1 activated the mitogen-activated protein kinase (MAPK) pathway, and inhibition of MAPK/Erk kinase inhibited virus entry. Entry was also blocked by dimethylamiloride, indicating that HIV-1 enters endothelial cells by macropinocytosis. Therefore, HIV-1 penetrates BMVECs in ICAM-1-lined macropinosomes by a mechanism involving lipid rafts, MAPK signaling, and glycosylaminoglycans, while CD4 and chemokine receptors play limited roles in this process.

Human immunodeficiency virus (HIV) enters the central nervous system (CNS) early after the primary infection (2, 45). Despite extensive investigation of HIV type 1 (HIV-1) neuroinvasion, the mechanisms of initial entry into the CNS remain obscure. "Trojan" transport of the virus by monocytes across the blood-brain barrier (BBB) is considered to have crucial importance for HIV-1 import into the CNS in the late stage of AIDS (26). However, early after the primary infection, monocytes are generally not infected (32). The two most likely sources of the initial neuroinvasion are infected $CD4^+$ lymphocytes and cell-free virions, both reaching high levels before the development of the anti-retroviral immune response.

Under normal conditions, the mammalian BBB presents a strong barrier to invasion of the CNS by microbial agents. This barrier is based on (i) paucity of vesicular activity within the brain microvascular endothelial cells (BMVECs) that limits endocytosis and transcytosis and (ii) tight junctional complexes that are, however, modulated by vasoactive substances, such as thrombin and bradykinin (52), and cytokines, such as tumor necrosis factor alpha (11). In disease states, fluid phase transcytosis may dramatically increase via vesiculocanalicular structures and organelles, and the BBB becomes less restrictive for blood-borne proteins and cells (27). The paracellular passage may also increase through gaps in tight junctions, which are produced by proinflammatory cytokines, such as tumor necrosis factor alpha (18), interleukin-1 (IL-1), and IL-6 (11).

HIV-1 enters susceptible cells by fusion of its envelope with the plasma membrane after binding to the CD4 molecule (9) and interaction with the chemokine coreceptor CXCR4 or CCR5 (51). The entry of HIV-1 into susceptible cells is pH independent (33), arguing against endosomal entry of HIV-1 into productively infected cells. However, unlike receptor-dependent uptake in productively infected cells, in abortive interactions, the virus is taken in by vesicular uptake (30) mediated by macropinocytosis (31).

Low-density, detergent-insoluble membrane fractions known as rafts that are rich in glycosphingolipids, sphingomyelin, cholesterol, glycosylphosphatidylinositol (GPI)-anchored proteins, and various signaling molecules (50) have been found to serve as receptors for a number of pathogenic microorganisms, including HIV-1 (15). The rafts organize gp120/gp41, CD4, and an appropriate chemokine coreceptor into a membrane fusion complex (23, 28), although a shift of raft-associated CD4 to CXCR4 located outside of the raft domain may be necessary

* Corresponding author. Mailing address: UCLA, CVRL, MRL 3645, 675 Young Dr. South, Los Angeles, CA 90095-1760. Phone: (310) 206-6392. Fax: (310) 825-1678. E-mail: fiala@ucla.edu.

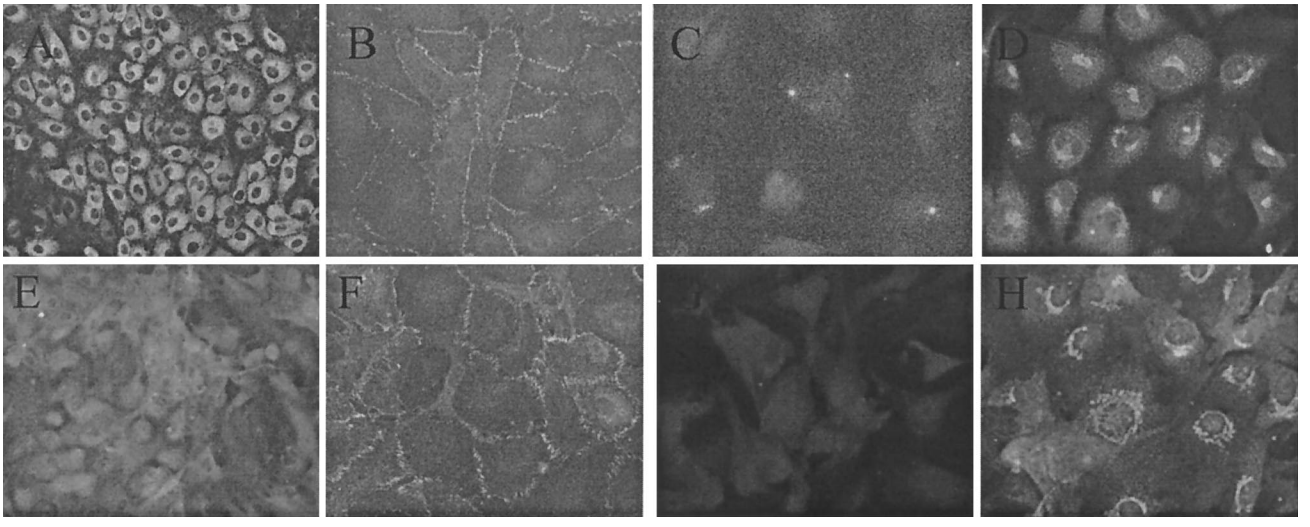

FIG. 1. Expression of cell markers on BMVECs and HUVECs. Primary HUVECs (A to D) and BMVECs (E to H) were cultured on gelatin-coated coverslips and stained by an indirect-immunofluorescence technique using anti-von Willebrand factor (A and E), anti-ZO-1 (B and F), anti-GLUT-1 (C and G), and anti-dynamin (D and H). (Magnification, ×400.)

for the fusion to occur (24). Lipid rafts also serve to correctly assemble the HIV-1 envelope during viral morphogenesis (35).

Retroviruses use several different mechanisms to traverse the BBB depending on the host and the virus. The simian immunodeficiency virus infection of simian brain endothelia was found to be productive (29), whereas the outcome of HIV-1 infection of human BMVECs in vitro has been controversial (34, 40). HIV-1 DNA was found within human brain endothelia (1), and visna virus DNA was detected in sheep brain endothelia (21). The in vivo analysis of HIV-1 brain infection is complicated by the Trojan transport of the virus in monocytes/macrophages and T cells. The Trojan transport by monocytes has been described for visna virus, feline immunodeficiency viruses, simian immunodeficiency virus, and HIV-1 (21), and Trojan transport by lymphocytes was demonstrated for human T-cell leukemia virus type 1 (46). In a mouse model, the transport of enveloped HIV-1 pseudovirions across the mouse BBB is related to adsorptive endocytosis of gp120 (3).

To investigate subcellular and molecular aspects of HIV-1 neuroinvasion, we developed an in vitro BBB model constructed with primary human BMVECs with or without astrocytes (18). In this model, cytokines, such as tumor necrosis factor alpha (18), and abused drugs, such as cocaine (54), open a paracellular route for HIV-1. Cell-free HIV-1 enters and penetrates coronary artery endothelial cells in cytoplasmic vacuoles (22). In the present work, we elucidate the mechanisms regulating virus entry into BMVECs.

TABLE 1. Exposure of BMVEC to HIV-1 does not increase permeability in the BBB model[a]

Virus exposure	Permeability coefficient (cm/min)[b]		
	4 h p.i.[c]	24 h p.i.[d]	48 h p.i.[e]
No	0.000194, 0.000244	0.000326, 0.000264	0.000178, 0.000186
Yes	0.000234, 0.000275	0.000298, 0.000295	0.000186, 0.000193

[a] Duplicate BBB models were either exposed in the upper chamber to HIV-1_{LAI} (1 million RNA copies) or left uninfected. At the indicated times, [^{14}C]inulin (20 μl; 25,000 to 30,000 cpm) was added for 1 h, and the permeability coefficient was determined as described in Materials and Methods.

[b] Values for duplicate experiments are shown.

[c] Mean difference, 0.00004; standard error of the difference, 0.00006; P = 0.5982.

[d] Mean difference, 0.00000; standard error of the difference, 0.00006; P = 0.9820.

[e] Mean difference, 0.00001; standard error of the difference, 0.00006; P = 0.9103.

MATERIALS AND METHODS

Cell culture. The University of Arizona Institutional Review Board for Research involving Human Subjects approved isolation of BMVECs from discarded temporal lobe tissues (5 to 15 mm^3) obtained at temporal lobectomies. The tissue was placed in phosphate-buffered saline (PBS) and fragmented using a 16-gauge needle. After centrifugation (300 × g for 5 min), the pellet was digested in a 20-ml solution of collagenase-dispase (1 mg/ml; Roche Molecular Biochemicals, Indianapolis, Ind.) containing 200 μl of DNase (1 mg/ml; Sigma, St. Louis, Mo.) and 20 μl of *N*α-*p*-tosyl-L-lysine chloromethyl ketone (0.147 mg/ml; Sigma) for 1 h at 37°C. The digest was spun down (1,000 × g for 20 min) and resuspended

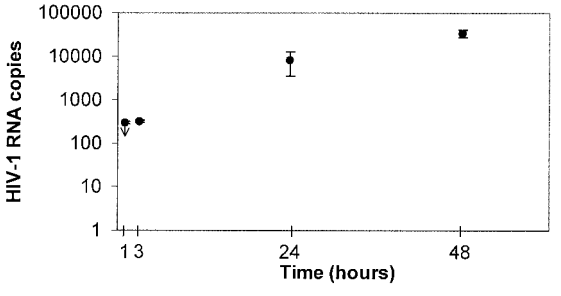

FIG. 2. Time course of HIV-1 penetration across the BBB model. One million HIV-1_{JR-FL} RNA copies were placed in the upper chambers of replicate BBB models, and HIV-1 penetration into the lower chambers was measured by a HIV-1 RNA (Amplicor) assay. On the vertical axis are shown the titers in the lower chamber (mean ± standard error of the mean) at the indicated times (the titer at 1 h p.i. was below the limit of detection [<300 RNA copies]). The infectious assay showed that at 48 h p.i., the titers were $>10^{-3}$ $TCID_{50}$ in the upper chamber and $10^{-1.3}$ $TCID_{50}$ in the lower chamber. The experiment was repeated three times with comparable results.

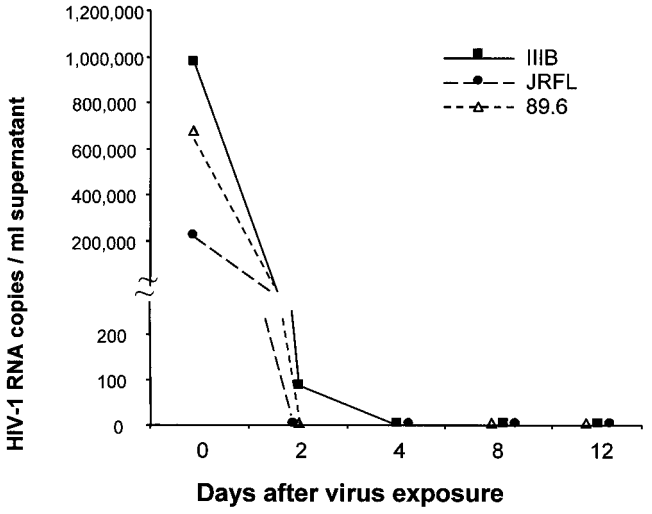

FIG. 3. HIV-1 does not replicate in BMVECs. The indicated number of HIV-1_{IIIB}, HIV-1_{JR-FL}, or HIV-$1_{89.6}$ RNA copies was placed on 200,000 BMVECs for 2 h, washed four times, and incubated for the indicated time, after which the supernatant was collected and HIV-1 RNA was measured by the Amplicor PCR assay. HIV-1_{IIIB}, HIV-1_{JR-FL}, and HIV-$1_{89.6}$ virus stocks were titrated in CEM lymphoblastoid cells and yielded p24 antigen in the range of 10^4 to 10^5 pg/ml.

in 20 ml of a bovine serum albumin solution (250 mg/ml). After a repeat centrifugation, the pellet containing capillaries was resuspended in 1 ml of PBS with bovine serum albumin (5 mg/ml) and loaded onto a 50% Percoll gradient. The capillary fragments were removed and placed in a three-dimensional collagen type I gel and maintained in Dulbecco's minimum essential medium-Ham's F12 with 10% fetal bovine serum with endothelial cell growth supplement (Sigma) added at 50 μg/ml as described previously (18). The microvessels were harvested, explanted into collagen type I-coated T-25 flasks, and propagated as monolayers. Coronary artery endothelial cells (CAECs) were obtained from Clonetics/BioWhittaker, Walkersville, Md., and propagated as described previously (22). Human umbilical vein endothelial cells (HUVECs) were provided by A. Burns, Baylor University, Houston, Tex., and were propagated as described previously (5).

Viruses. The following HIV-1 strains were used for investigations. (i) Two R5-tropic strains, HIV-1_{JR-FL} (I. Chen, University of California—Los Angeles) and HIV-1_{ADA} (20) (H. Gendelman, Walter Reed); four X4-tropic strains, HIV-1_{NL4-3} (R. Gallo, University of Maryland), HIV-1_{MN} (R. Gallo), HIV-1_{LAI} (L. Montagnier, Pasteur Institute), and HIV-1_{IIIB} (R. Gallo); and a bitropic strain, HIV-$1_{89.6}$ (J.-M. Bechet and R. Colman). All of these strains were provided by the AIDS Research and Reference Reagent Program, NIAID, NIH. (ii) For reverse transcription, HIV-1_{LAI} was used. (iii) For transmission electron microscopy (TEM) of virus entry, HIV-1_{LAI} was used. (iv) For virus signaling, HIV-1_{MN} (J. Lifson and L. Arthur, SAIC, Frederick, Md.) was used, including an active (infectious) virus preparation containing 460,000 50% tissue culture infective doses ($TCID_{50}$) per ml, vaccine virus inactivated by aldrithiol (47), and vesicles from uninfected cells (these products were prepared identically by ultracentrifugation in a sucrose density gradient and had comparable concentrations of protein [active virus, 2.56 mg/ml; inactivated virus, 2.97 mg/ml; vesicles, 1.49 mg/ml]). (v) For confocal microscopy of virus entry, HIV-1_{NL4-3} was used by transfecting 293T cells with DNA of the infectious molecular clone (43). HIV-1_{NL4-3} incorporating Vpr-green fluorescent protein (GFP) (HIV-1_{NL4-3} Vpr-GFP) was used by cotransfection of 293T cells with pNL4-3 DNA and an expression vector coding for GFP-Vpr fusion protein. Forty-eight hours after transfection, the culture supernatants were collected, filtered through a 0.45-μm-pore-size filter, and concentrated by ultracentrifugation through a cushion of 20% sucrose in PBS. The pelleted virus was resuspended in PBS with 0.1% bovine serum albumin, aliquoted, and stored frozen at −80°C. The virus titer was determined by the reverse transcriptase activity assay (44); the GFP-Vpr expression vector was constructed by PCR amplification of the coding region of HIV-1 Vpr (HIV-1 YU2) from the pTM-vpr1 vector (53) and cloning into *Xho*I and *Eco*RI sites of pEGFP-C1 (Clontech Laboratories, Palo Alto, Calif.). A pseudotyped luciferase-expressing NL HXB2 Env^+ LUC^+ virus was obtained by cotransfection of plasmid DNA (15 μg) encoding envelope from a T-tropic HIV-1 clone, HXB2, and pNL4-3 Env^- LUC^+ (5 μg) into 293T cells using SuperFect (Qiagen). The virus GFP-HIV-1_{NL4-3} Env^- was created by cotransfection of GFP-Vpr and HIV-1_{NL4-3} Env^- plasmid (provided by O. Schwartz, Pasteur Institute, Paris, France) in 293 T cells. All HIV-1_{NL4-3} viruses except GFP-HIV-1_{NL4-3} Env^- were infectious in T cells and had comparable titers by a reverse transcriptase assay (2.5×10^7 to 1×10^8 cpm/ml).

In the luciferase assay, the cells were infected with NL HXB2 Env^+ LUC^+, and at specified times, the cells were washed and lysed using the Luciferase Cell Culture Lysis Reagent (Promega). The lysate was collected and centrifuged, and the supernatant was stored frozen until it was used in the assay with the luciferase assay reagent and for scintillation counting using a Monolight 2010 luminometer (41). A HIV-1 infectious end point assay was performed in A3.01 cells as described previously (18).

Antibodies, probes, and inhibitors. The following primary antibodies were used: anti-von Willebrand factor (DAKO, Carpenteria, Calif.); anti-ZO-1 (Zymed, South San Francisco, Calif.); anti-phospho-extracellular signal-regulated kinases 1 and 2 (Erk 1 and 2; Cell Signaling Technology, Beverly, Mass.); anti-glucose transporter-1 (GLUT-1) and anti-GAPDH (glyceraldehyde-3-phosphate dehydrogenase) (Chemicon International, Temecula, Calif.); anti-caveolin-1 (Santa Cruz Biotechnology, Santa Cruz, Calif.); monoclonal anti-human ICAM-1 (DAKO); and monoclonal anti-HIV-1 p24 (183-H12-5C) and monoclonal anti-Tat (8D1.8) (AIDS Research and Reference Reagent Program).

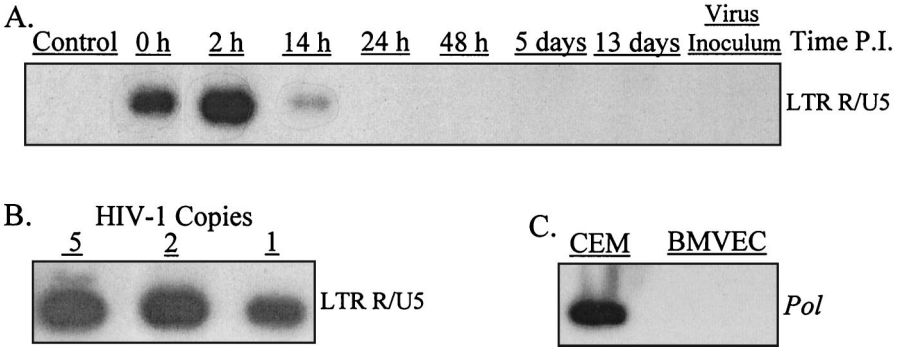

FIG. 4. HIV-1 reverse transcription in BMVECs proceeds to LTR/U5. (A) Replicate BMVEC cultures (400,000 cells in 60-mm-diameter tissue culture dishes) were infected with 10^6 RNA copies of HIV-1_{LAI} (100 pg of p24 antigen) for 2 h at 37°C and washed four times with PBS. The cells were harvested using 0.25% trypsin–1 mM EDTA at the indicated times p.i. The cell lysates were subjected to PCR amplification using the primers from the LTR/U5 region, the *pol* gene, or 2LTR circles. The hybridization was positive only with the LTR/U5 probe; the hybridizations with the probe for *pol* or 2LTR circles were negative. (B) Dilutions of PCR lysates prepared from 8E5/LAI cells containing one HIV-1 provirus per cell were amplified with the same set of primers used for panel A. (C) Cell lysates from CEM lymphoblastoid cells or BMVECs infected with HIV-1 for 9 days were subjected to PCR amplification using the primers from the *pol* gene.

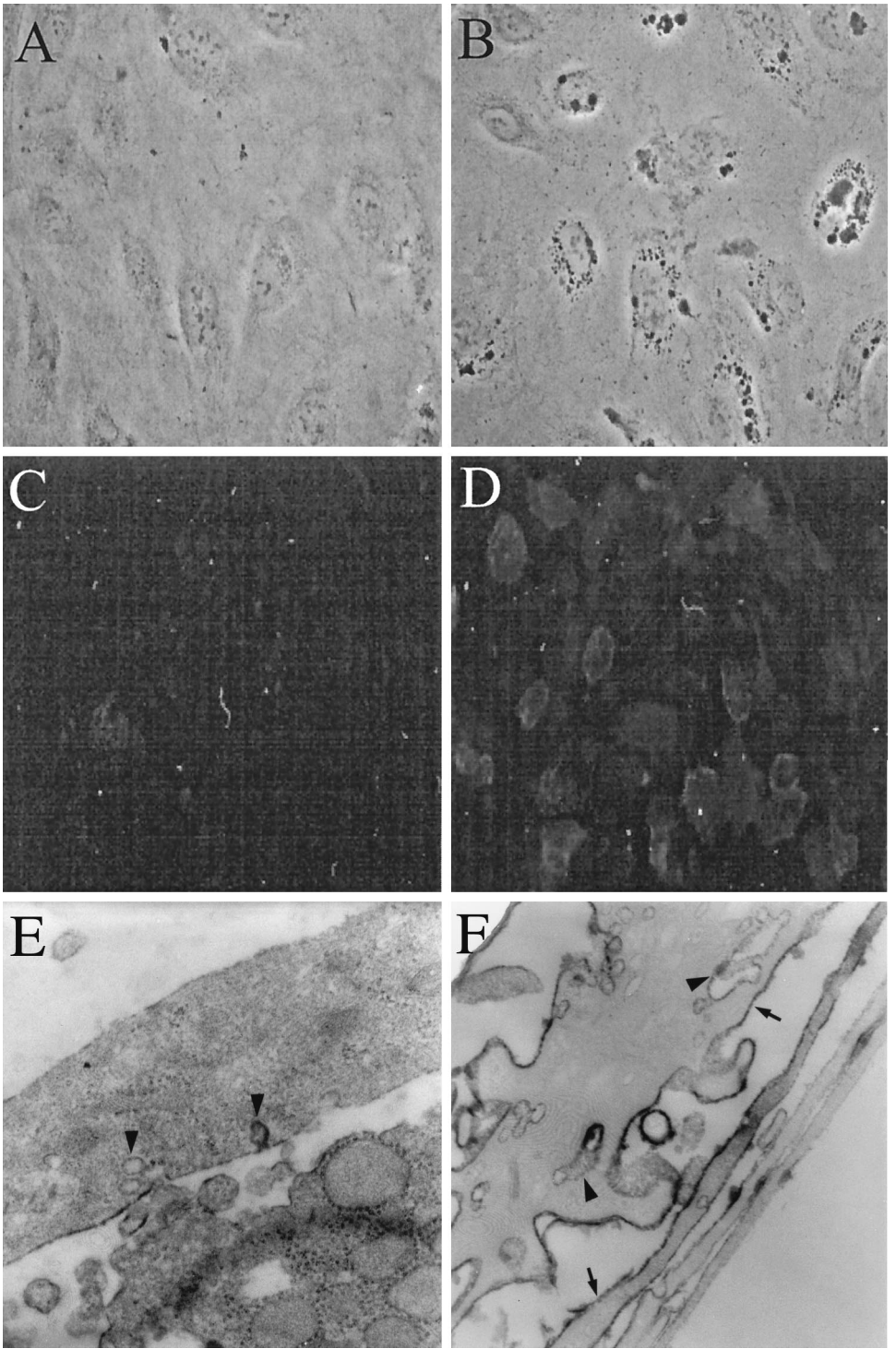

FIG. 5. HIV-1 exposure of BMVECs induces ICAM-1 on plasma membranes and in cytoplasmic vacuoles. BMVECs, sham inoculated or inoculated with HIV-1 at a multiplicity of 10^5 RNA copies per cell, were fixed at the indicated times and examined by phase-contrast, fluorescence, or electron microscopy. (A) Control BMVECs show no cytoplasmic vacuoles (3 h post-sham infection; phase-contrast microscopy; magnification, ×100). (B) Virus-exposed BMVECs display cytoplasmic vacuoles (3 h p.i.; phase-contrast microscopy; magnification, ×100). (C) Control BMVECs display no ICAM-1 (24 h p.i.; anti-ICAM immunofluorescence; magnification, ×40). (D) HIV-1-exposed BMVECs strongly display ICAM-1 on the plasma membrane (24 h p.i.; anti-ICAM immunofluorescence; magnification, ×40). (E) Control BMVECs show no or weak ICAM-1 horseradish peroxidase (HRP) reaction product on the plasma membrane (arrowheads) (3 h post-sham infection; IEM with anti-ICAM-1; magnification, ×17,000). (F) Virus-exposed BMVECs display strong ICAM-1 HRP reaction product on the plasma membrane (arrows) and within vesiculocanalicular cytoplasmic structures (arrowheads) (3 h p.i.; IEM with anti-ICAM-1; magnification, ×17,000).

Texas Red (TR)-conjugated goat anti-rabbit immunoglobulin G and Alexa 488-conjugated goat anti-mouse immunoglobulin G, LysoTracker Red, and transferrin-TR were from Molecular Probes (Eugene, Oreg.). Cyclodextrin, nystatin, dimethylamiloride, and heparin were from Sigma.

HIV-1 invasion in a BBB model. The BBB models were prepared in Biocoat cell culture inserts (Collaborative Biomedical Products, Bedford, Mass.) using 40,000 BMVECs on the upper surface of a polyethylene teraphthalate membrane coated with fibronectin and collagen I, as described previously (18). The models were used on the fourth day after being plated, when the average [^{14}C]inulin permeability coefficient was 0.000219 cm^2/min.

To investigate the time course of HIV-1 invasion, we placed 10^6 RNA copies of HIV_{JR-FL} into the upper chamber of each model and counted the HIV-1 RNA copies in the lower chamber at various times. To examine virus invasion by TEM, HIV-1_{MN} (10 μl) was placed into the upper chamber of the BBB model. Replicate models were fixed at the appropriate times for 1 h at room temperature with 3% glutaraldehyde in PBS.

PCR analysis of HIV-1 reverse transcription products. BMVECs (400,000) were exposed to 1 million RNA copies of HIV-1_{LAI} that had been pretreated with 400 U of RNase-free DNase I (Boehringer Mannheim)/ml in PBS containing 0.04 M $MgCl_2$ (for 1 h at room temperature). After 4 h of incubation with the virus, the cells were washed four times with PBS and further cultivated. At various time intervals after infection, the cells were scraped and centrifuged, and the cell pellet was frozen. After thawing, the cell pellets were lysed in 200 μl of PCR buffer. Following protein digestion (for 2 h at 56°C) and inactivation of proteinase K (for 10 min at 95°C), 25 μl of cell lysate was subjected to 35 cycles of amplification as described elsewhere (49). The primers for long terminal repeat (LTR) R/U5 were 5′-GGC TAA CTA GGG AAC CCA CTG-3′ (forward) and 5′-CTG CTA GAG ATT TTC CAC ACT GAC-3′ (reverse); those for *pol* were 5′-TTC TTC AGA GCA GAC CAG-3′ (forward) and 5′-ACT TTT GGG CCA TCC ATT-3′ (reverse). To evaluate the sensitivity of each primer pair, different dilutions of the lysate prepared from 8E5/LAI cells (containing one copy of the HIV-1 genome per cell) were amplified in parallel. The amplified DNA was analyzed by Southern blot hybridization with ^{32}P-labeled probes (49).

HIV RNA copy (Amplicor) assay. HIV-1 viral RNA in culture supernatants was measured using the Amplicor HIV Monitor test kit (Roche Co., Nutley, N.J.) as described previously (18). The lower limit of sensitivity is 300 RNA copies (approximately 0.03 pg of p24/ml).

HIV-1 p24 antigen assay. A HIV-1 p24 enzyme-linked immunosorbent assay (ELISA) kit (NEN Life Science Products, Boston, Mass.) was used with QuantiKin software and Elast signal amplification according to the manufacturer's directions (sensitivity, 7 pg of p24/ml).

Western blotting. BMVECs were grown in 60- by 15-mm culture plates. After reaching 80% confluence, approximately 1 million cells were maintained overnight in EBM-2 basal medium (Clonetics/BioWhittaker) with 0.5% fetal bovine serum. The next day, the cells were stimulated for 5 or 15 min by addition of prewarmed spent medium with an equal volume (10 μl) of either the virus or control vesicles. The medium was then replaced with 200 μl of ice-cold cell lysis buffer (1% Triton X-100, 50 mM HEPES [pH 7.4], 100 mM NaCl, 10% glycerol, 5 mM $MgCl_2$, 1 mM EGTA, 10 μg of aprotinin/ml, 10 μg of leupeptin/ml, 1 mM orthovanadate, 50 mM sodium fluoride, and 20 mM β-glycerophosphate), and the lysate was incubated on ice for 30 min. After centrifugation (18,000 × *g* for 15 min), the lysates were frozen at −80°C.

Equal amounts of protein (25 to 50 μg) from each sample were loaded onto 7.5% sodium dodecyl sulfate–acrylamide Ready Gel (Bio-Rad, Richmond, Calif.) and separated using the Mini-Protean 3 electrophoresis system. The separated proteins were transferred to polyvinylidene difluoride membranes (Amersham-Pharmacia Biotech, Piscataway, N.J.) using the Trans-blot SD semidry electrophoresis transfer cell (Bio-Rad) and were incubated with primary and secondary horseradish-peroxidase-conjugated antibodies. The autoradiograms were developed by enhanced chemiluminescence using the ECL Western blotting detection kit (Amersham Pharmacia Biotech) and scanned using Eagle Eye II (Stratagene). The membrane was stripped in a detergent buffer (100 mM 2-mercaptoethanol, 2% sodium dodecyl sulfate, 62.5 mM Tris [pH 6.7]) and probed with anti-GAPDH to verify equal protein loading.

Immunocytochemistry, immunofluorescence, and confocal microscopy. BMVECs were grown for 3 days on gelatin-coated, glutaraldehyde-cross-linked coverslips and exposed to HIV-1_{NL4-3} Vpr-GFP for 3 h or overnight. To inhibit virus entry, the cells were treated with methyl-β-cyclodextrin or nystatin (Sigma). Immunocytochemistry was performed using the LSAB+ (peroxidase) kit (DAKO). For immunofluorescence analysis, the cells were fixed with 3% paraformaldehyde in PBS for 2 h at room temperature, treated with PBS–1% bovine serum albumin for 30 min at room temperature, permeabilized with 0.1% Triton, incubated overnight with one or two primary antibodies (monoclonal antibody at 10 μg/ml or polyclonal antibody diluted 1:200), washed three times with PBS, and incubated with one or two secondary antibodies (TR-conjugated goat anti-rabbit and Alexa 488-conjugated goat anti-mouse antibodies). Colocalization with cellular organelles was examined using Alexa Fluor 594-labeled transferrin and cholera toxin B, or T-R-labeled dextran (molecular weight, 40,000) and Lysotracker Red DND-99 (Molecular Probes). The preparations were examined using an Olympus Research BX60 microscope or a Zeiss LSM 310 confocal microscope.

TEM. Tissue culture inserts with membranes containing BMVEC monolayers were gently rinsed with PBS and fixed with 3% glutaraldehyde in 0.1 M sodium phosphate at pH 7.4 for 3 h at room temperature. Excess plastic was trimmed from the insert using flame-heated no. 11 scalpel blades. The membranes with attached cells were placed in an ice-cold buffer containing 0.2 M sucrose and 0.1 M sodium cacodylate at pH 7.4. The membranes were postfixed in 1 to 2% OsO_4 in 0.1 M sodium cacodylate buffer at 4°C for 1 h, dehydrated in a graded series of ethanol, cleared in propylene oxide, and placed in 100% liquid plastic. The individual membranes were cut from the inserts, bisected, and flat embedded in both Polybed 812 and Spurr plastics. Thick and thin sections were cut on a Reichert or LKM Ultramicrotome, stained with lead and uranyl acetate salts, and examined using a Zeiss EM 10 electron microscope.

Immunoelectron microscopy (IEM). For identification of ICAM-1, we applied a preembedding technique according to a previously described method (27). Inserts were fixed for 3 h with 4% formalin containing 0.25% glutaraldehyde in a 0.1 M sodium cacodylate buffer at pH 7.3. The inserts were quenched with 0.1 M NH_4Cl to remove unbound aldehydes and then blocked with 10% goat serum in PBS. The inserts were then immunoreacted with a mouse anti-human ICAM-1 (1:100), goat anti-mouse biotinylated immunoglobulin (1:50), streptavidin-horseradish peroxidase (1:50), and finally 3,3′-diaminobenzidine tetra-HCl. The inserts were postfixed with 1 to 2% OsO_4 and processed into plastic, as described above.

Permeability coefficient. The permeability coefficient was assessed in the BBB model by a diffusion assay using 25,000 to 30,000 cpm of ^{14}C-carboxylated inulin (molecular weight, 5,000) (Sigma) in the upper chamber, as described previously (18).

Data acquisition. The imaging program Image Pro (Media Cybernetics, Silver Spring, Md.) measured green (GFP), red (cholera toxin), and yellow (colocalization) areas in three cells in confocal images obtained with a 100× objective of the confocal microscope.

The Global Image Analysis package (Data Translation, Inc.) was used to measure the areas (pixels) of the cytoplasmic vacuoles with viral particles and viral remnants relative to the total endothelial cell area based on electron micrographs examined at ×12,189 magnification.

Statistical analysis. The permeability coefficient data were analyzed by repeated-measures analysis of variance with the posthoc *t* test. The areas of cytoplasmic vesicles at 3 and 16 h were analyzed by the Wilcoxon rank sum nonparametric test.

RESULTS

In previous studies, we investigated HIV-1 invasion in a BBB model constructed with BMVECs on a porous membrane (18) and observed that BMVECs represent the main barrier to HIV-1 invasion, which is not altered by the presence of an astrocyte sublayer.

Cell markers and chemokine coreceptors are displayed on BMVECs in tissue-specific fashion. We compared cell markers on BMVECs to those described previously on HUVECs (5, 22). BMVECs and HUVECs showed substantial differences in the expression of factor VIII, GLUT-1, and dynamin (Fig. 1). As described previously, the chemokine receptor distribution on endothelial cells in vitro is tissue specific: CXCR4 was expressed on BMVECs, CAECs, and HUVECs; CCR5 was expressed on CAECs and BMVECs; CCR3 was expressed only on BMVECs, as previously described (5).

A small fraction of the virus inoculum penetrates the BMVEC barrier despite no alteration of paracellular permeability. To assay virus invasion across the BBB, HIV-1 inoculum (10^6 RNA copies, an amount comparable to the virus load

in the plasma of infected patients early after infection) was placed in the upper chamber of the BBB model. The concentration of the virus was measured by a sensitive HIV-1 RNA (Amplicor) assay and an infectious assay in the upper and lower chambers. The RNA assay showed that the invasion was initially (1 to 3 h postinfection [p.i.]) minimal but slowly increased (Fig. 2). The infectious assay revealed that the virus titer 48 h p.i. in the upper chamber was $>10^{-3}$ $TCID_{50}$ and that in the lower chamber was $10^{-1.3}$ $TCID_{50}$. During the 48-h test period, HIV-1 exposure did not significantly alter the paracellular permeability of replicate BBB models, as shown using a [^{14}C]inulin assay (Table 1).

Since the paracellular route was not breached by HIV-1 exposure, we investigated two alternative possibilities: HIV-1 penetration by replication in BMVECs and a transcellular pathway.

HIV-1 does not replicate in BMVECs. To determine whether HIV-1 invasion could take place by virus replication and budding on the abluminal side of brain endothelia, we performed PCR, ELISA, immunofluorescence, and luciferase assays with HIV-1-exposed BMVECs. Replicate BMVEC monolayers (2×10^5 cells) were exposed to the macrophage-tropic strains JR-FL and ADA, the T-cell-lymphotropic strains IIIB and LAI, or the dual-tropic strain 89.6 (300,000, 700,000, and 1,000,000 RNA copies, respectively), and after thorough washing, viral RNA and p24 antigen were measured in the supernatant up to 12 days p.i. Except for the release of 89 copies of IIIB on day 2, no HIV-1 RNA was released at any time from virus-exposed BMVECs (Fig. 3). Furthermore, we did not detect on days 3 and 7 p.i. any intracellular p24 or Tat by immunofluorescence or p24 antigen in the supernatant medium by ELISA. Finally, we measured the luciferase activities of lysates from BMVECs which had been either pretreated or not pretreated with bacterial lipopolysaccharide (100 ng/ml) and exposed to luciferase-expressing recombinant virus, NL HXB2 Env^+ LUC^+, for different periods of time (4 or 7 days). The luciferase activity did not rise significantly above the background in any sample (the maximum activity was 153 relative light units). A positive infection generates at least 10^3 relative light units (41).

These experiments demonstrated that HIV-1 does not productively infect human BMVECs isolated from the microvessels in the temporal lobe. To further clarify the nature of virus interactions with BMVECs, we examined the sequential steps in HIV-1 reverse transcription.

HIV-1 reverse transcription in BMVECs is restricted to R/U5 transcripts. In BMVECs exposed to HIV-1_{LAI}, an early transcript, strong-stop DNA R/U5, was detected 0, 2 (maximum), and 14 h p.i. but not at later times (Fig. 4A). Reverse transcription of U3/R and *pol* was not detected in BMVECs (but was positive in CEM lymphoblastoid cells [Fig. 4C]). Analysis of BMVEC infection by HIV-$1_{JR\text{-}FL}$ and HIV-$1_{89.6}$ strains produced identical results. We considered the possibility that the observed PCR signal could reflect endogenous reverse transcription. However, we did not detect any R/U5 transcripts in the viral inoculum (Fig. 4A). The data, therefore, suggested that a low level of R/U5 transcription occurs very early after virus entry into BMVECs; these reverse transcriptase products disappeared at later times. Viral reverse transcription beyond the R/U5 step did not occur.

These findings indicated that HIV-1 does not replicate in BMVECs. We therefore examined the remaining possibility: transcellular transport of HIV-1.

HIV-1 upregulates the expression of ICAM-1 on the plasma membrane and in cytoplasmic vacuoles. Three hours p.i., HIV-1-exposed, but not control, BMVECs displayed robust vacuolization, as visualized by phase-contrast microscopy (compare Fig. 5A and B), and 24 h p.i., cells showed increased expression of ICAM-1 when examined by immunofluorescence microscopy (compare Fig. 5C and D) or IEM (compare Fig. 5E and F). Control cells demonstrated only weak ICAM-1-specific staining (a horseradish peroxidase-positive reaction product) on the external plasma membrane (Fig. 5E), whereas virus-exposed cells displayed abundant staining both on the plasma membrane and in cytoplasmic vesicles (Fig. 5F). In addition, 16 h p.i., HIV-1-exposed endothelial cells displayed increased rough endoplasmic reticulum when examined by TEM (see Fig. 7B).

To clarify the entry and passage of HIV-1 through BMVECs, we performed TEM and confocal microscopy.

HIV-1 enters BMVECs by vesicular uptake and is lysed after the fusion of vesicles with lysosomes. Three hours p.i., virus-exposed cells had strongly increased cell surface microvilli trapping many virions, which were taken into cytoplasmic vesicles through surface invaginations. The incoming virions did not show fusion of the virus envelope with the cell membrane (Fig. 6A and B). Most virions entered through non-clathrin-coated invaginations, but an occasional virion entered through a clathrin-coated pit (Fig. 6C). The vesicles were of various sizes (150 nm to 5 μm in diameter) and incorporated from a single virion to as many as thousands of virions. An occasional giant vesicle spanned almost the whole cell width (Fig. 7A). At 16 h p.i., most virion-containing vesicles had fused with primary lysosomes, and the virions in these vesicles disappeared. The virions remained intact in occasional vesicles that did not fuse with lysosomes (Fig. 7C). In order to show the evolution of these cytoplasmic vesicles over time, the area of vesicles expressed as a fraction of the total endothelial cell area was determined in three cells. This value was significantly higher at 3 h p.i. (25.34%) than at 16 h p.i. (4.95%) (Table 2). The TEM results demonstrating the virus in the cytoplasmic vesicles were supported by confocal microscopy (see below).

Virus colocalizes on entry with the ganglioside GM1, and this entry is inhibited by cholesterol removal and heparin. To analyze the mode of virus entry into BMVECs, we employed HIV-1 carrying GFP-Vpr fusion protein (HIV-$1_{NL4\text{-}3}$ Vpr-GFP). HIV-1-GFP did not colocalize on entry with transferrin, the marker of early endosomes (Fig. 8C), but colocalized extensively with cholera toxin B, which targets GM1 ganglioside in lipid rafts (Fig. 8A). The intensity of colocalization of the virus with cholera toxin B varied from cell to cell, probably reflecting asynchrony in virus entry.

Both the sterol binding agent methyl-β-cyclodextrin (19) and the antifungal antibiotic nystatin, which extracts cholesterol from caveolae (8), inhibited the entry of HIV-1-GFP and cholera toxin B into BMVECs and their colocalization (Fig. 8A), supporting the role of lipid rafts in virus entry.

Virus entry was completely blocked by the pharmaceutical polysaccharide heparin (Fig. 8B), suggesting that HIV-1 is binding to cell membrane-bound proteoglycans. Previously, a

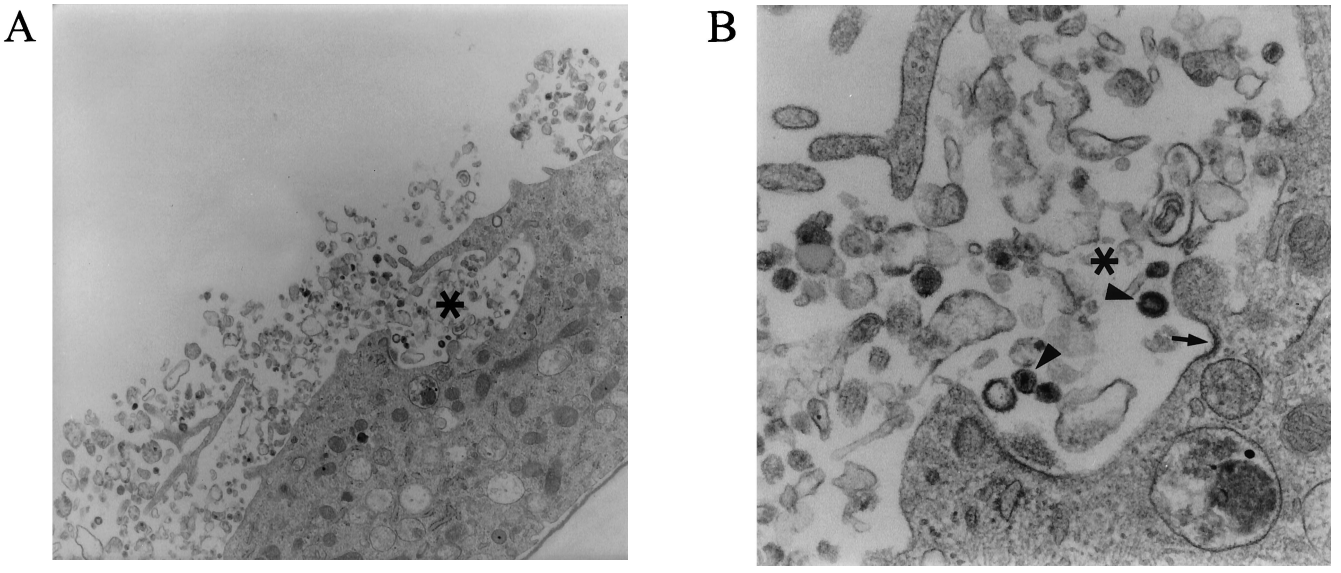

FIG. 6. HIV-1 virions enter BMVECs through a surface crater. BMVECs were exposed to HIV-1 at a multiplicity of 10^5 RNA copies per cell, fixed at the indicated times, and examined by TEM. (A) At 3 h p.i., exuberant microvilli trap virions on the cell surface and in a large surface crater (asterisk). (Magnification, ×5,670.) (B) A higher magnification of panel A shows numerous virions (arrowheads) in a large surface crater (asterisk). A portion of the crater is clathrin coated (arrow). (Magnification, ×36,000.) (C) An occasional viral particle enters a clathrin-coated pit (arrow). (Magnification, ×60,000.)

nonproductive interaction of HIV-1 with macrophages was described (30, 48). Since this interaction involved HIV-1 entry into macrophages by vesicular uptake that did not depend on CD4 or chemokine receptors, we investigated whether HIV-1 entry into BMVECs employs a similar mechanism.

HIV-1 entry into BMVECs does not depend on gp120, CD4, or CCR5 but proceeds via macropinocytosis. Upon exposure of BMVECs to HIV-1_{NL4-3} Vpr-GFP Env^+ or GFP-HIV-1_{NL4-3} Env^-, the virus entered the cells; however, the entry of the envelope-positive virus was more efficient than the entry of the envelope-deficient construct (Fig. 8B). HIV-1 entry was not dependent on the classical receptors for HIV-1, since CD4 antibody had no effect and RANTES had only a small inhibitory effect on virus entry (Fig. 8B). Virus entry was, however, inhibited by the Na^+-K^+ transporter inhibitor dimethylamiloride (Fig. 8B), indicating that endocytic uptake of the virus occurs by macropinocytosis. As expected from this mode of entry, virus colocalized with the fluid marker dextran but not with transferrin (Fig. 8C).

After entry into vesicles, the virus was lysed in those vesicles that fused with lysosomes (Fig. 7C). HIV-1_{NL4-3} Vpr-GFP Env^+ showed a minimum colocalization with the Lysotracker probe for lysosomes (Fig. 8C), indicating a very short half-life of the virus in this compartment. The virus weakly colocalized with caveolae (Fig. 8C).

To investigate the role of virus-induced signaling in HIV-1 entry, we examined induction of Erk 1 and 2 phosphorylation in BMVECs.

HIV-1 activates the MAPK pathway, which is essential for virus entry. The exposure of BMVECs to HIV-1_{MN} increased Erk 1 and 2 phosphorylation 1.5 times 5 min p.i. and 3.4 times 15 min p.i. compared to a control vesicle preparation from uninfected cells (Fig. 9). The MEK inhibitor U0126 strongly suppressed virus-induced Erk 1 and 2 phosphorylation (data not shown) and virus entry (Fig. 8A). These results suggest that Erk 1 and 2 activation by the virus is required for efficient entry into BMVECs.

DISCUSSION

The BBB has been widely considered to be an impenetrable barrier to HIV-1 which can be crossed by HIV-1 only by piggybacking in monocytes or lymphocytes (26). Here, we demonstrate that in vitro HIV-1 is initially held back by the BMVEC barrier, but within 3 h p.i., the virus is able to enter the endothelial cells, which display abundant cytoplasmic vesicles containing HIV-1 virions. The virus does not replicate or

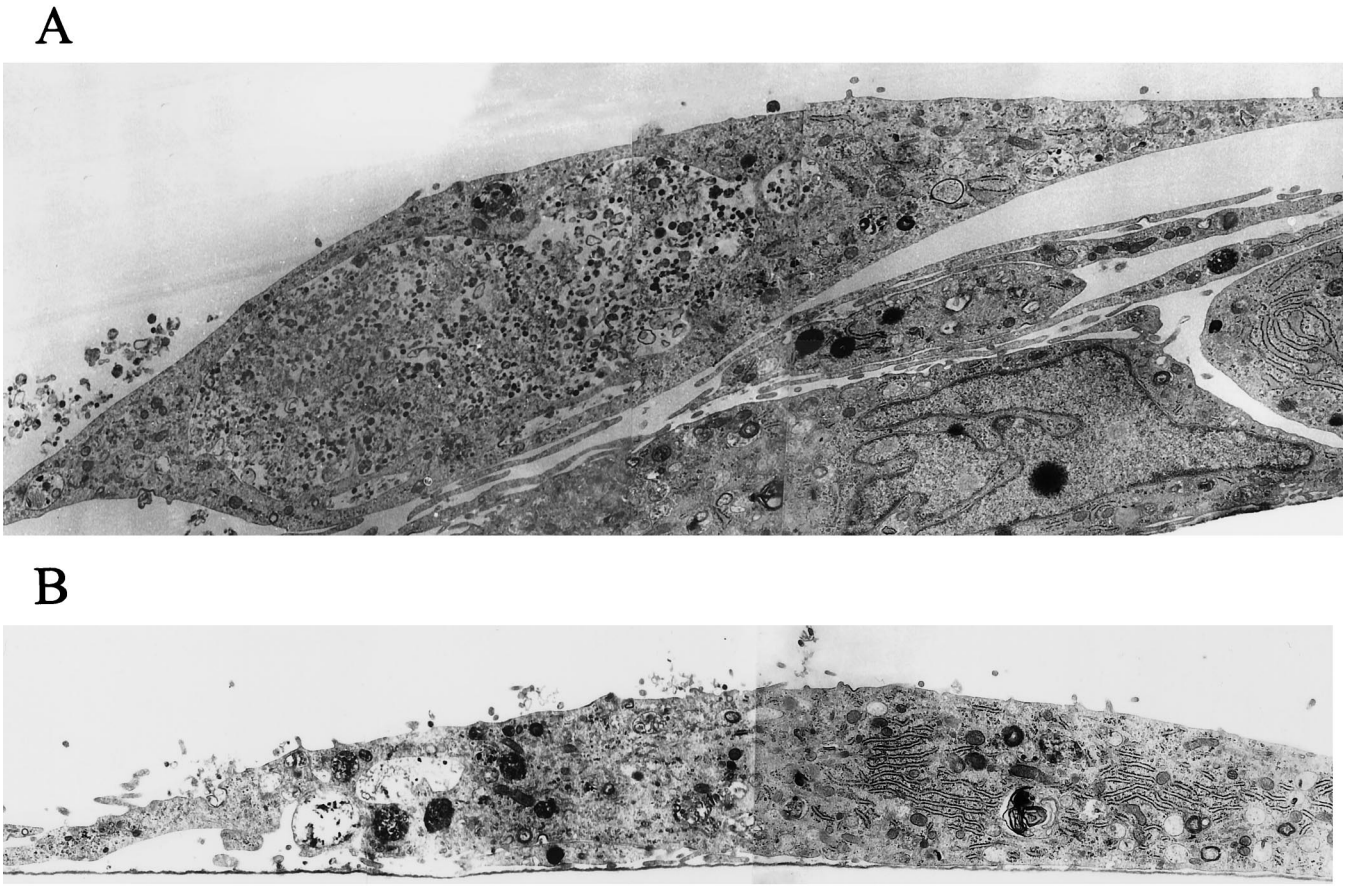

FIG. 7. Abundant cytoplasmic vesicles display virions early after infection, but subsequently the vesicles diminish and the virions disappear. BMVECs were infected with HIV-1 at a multiplicity of 10^5 RNA copies per cell, fixed at the indicated times, and examined by TEM. The montage of electron microscopic figures shows the typical appearance of whole cells 3 and 16 h p.i. (A) BMVEC (3 h p.i.) shows a giant vacuole and several small vacuoles with virions (magnification, ×12,000). (B) BMVEC (16 h p.i.) shows only small vacuoles with amorphous virion remnants. Note the abundant rough endoplasmic reticulum (magnification, ×12,000). (C) BMVEC (16 h p.i.) shows amorphous virion remnants (arrow) in the vesicle that had fused with a lysosome (asterisk). The vesicle that had not fused with a lysosome contains intact virions (arrowhead) (magnification, ×30,000)

disrupt tight junctions, yet approximately 1% of the virus inoculum penetrates to the abluminal side of the BMVEC barrier.

The entry of HIV-1 into susceptible T cells generally occurs by a pH-independent membrane fusion (7, 12) after interaction of the virus envelope with CD4 and chemokine coreceptors on the target cell (4). We show here that HIV-1 penetration across brain endothelia (and hence BBB) is not due to virus replication or virus penetration through a paracellular route. We demonstrate that virus enters BMVECs nonproductively via macropinocytosis, which is dependent on intact lipid rafts and MAPK signaling. The existence of a macropinocytotic mechanism of viral entry into BMVECs is supported by increased surface microvilli, abundance of cytoplasmic vesicles, and inhibition of virus entry by dimethylamiloride. The intracellular vesicles enclosing HIV-1 virions in BMVECs are of various sizes and do not strongly colocalize with the anticaveolin target, and therefore, they differ from the "caveosomes" recently described with simian virus 40 (37). As shown by TEM, the cytoplasmic vesicles fuse with lysosomes and become reduced in size, and most virions are lysed, corresponding to clearance of the virus from BMVECs and the culture supernatant. This nonproductive HIV-1 entry into the endothelial cell cytoplasm appears, as is the case with productive entry of HIV-1 into $CD4^+$ T cells (41), to be dependent on the integrity of lipid rafts.

The subcellular trafficking of HIV-1 in BMVECs appears to be largely terminated by fusion of endocytic vesicles with lysosomes, although the data in the BBB model show that approximately 1% of the virus penetrates the BMVEC monolayer. HIV-1 does not follow transferrin into recycling endosomes or GPI-GFP into the Golgi apparatus (36). HIV-1 invasion of BMVECs produced substantial endothelial restructuring, which could promote virus penetration to the abluminal side. The initial stimulus for cytoskeletal rearrangements in BMVECs could be transmitted through ICAM-1 engagement. Etienne-Manneville and coworkers showed that ICAM-1 cross-linking leads to cytoskeletal endothelial restructuring through tyrosine phosphorylation of phosphatidylinositol-phospholipase Cγ1 (14). The adhesion molecule ICAM-1 also plays a key role in inflammatory cell homing and trafficking across normal and injured blood-tissue barriers, where it is highly expressed (10, 13). HIV-1-induced cell surface invaginations and tubulovesicular structures in HIV-1-exposed

C

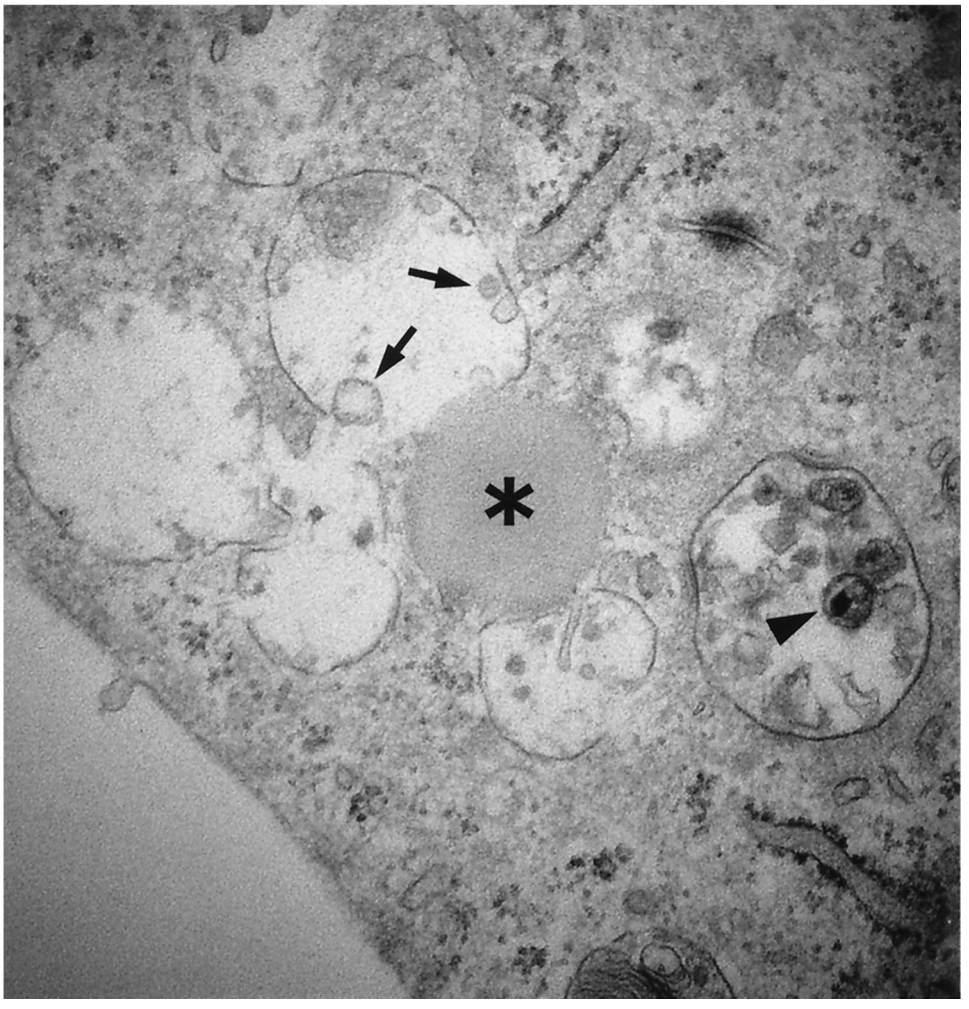

FIG. 7—*Continued.*

BMVECs were ICAM-1 lined and might correspond to ICAM-1-positive vesiculotubular structures in brain tumors (27). The profound subcellular alterations of endothelial cells exposed to HIV-1 could also be related to certain cytokines, including IL-6, which is secreted by HIV-1-exposed endothelial cells (25; M. Fiala, unpublished data), and vascular endothelial growth factor, which induces vesiculovacuolar organelles and transcellular pores in tumor vessels (16, 17).

Virus entry was dependent on the MAPK signaling pathway. This pathway has been recognized to play a role in the life cycles of other viruses, for example, during nuclear export of influenza virus (39) or the spread of Borna virus to adjacent cells (38). In T-cell lines, HIV-1 activates the MAPK pathway with induction of inflammatory cytokine genes (42). The cell receptor used by HIV-1 for MAPK signaling in BMVECs and CAECs is still unknown. Mammalian cell surfaces display membrane-bound proteoglycans that bind extracellular proteins and form signaling complexes with receptors (6). Since virus entry was inhibited by heparin, HIV-1 could be using a proteoglycan receptor for signaling in BMVECs. Although chemokine receptors are present on BMVECs and CAECs (5), HIV-1 does not appear to use these receptors for its entry because (i) virus invasion across CAECs is not inhibited by the broadly active chemokines AOP-RANTES and v-MIP-II (22) and (ii) the chemokine RANTES does not significantly block virus entry into BMVECs.

TABLE 2. Time-dependent decrease of intracytoplasmic vesicles in HIV-1-inoculated BMVECs

EC examined[a]	Area of vesicles/area of EC (in pixels) (%)	
	3 h p.i.[b]	16 h p.i.[b]
EC 1	10,435/78,840 (13.2)	3,420/47,029 (7.27)
EC 2	41,466/78,369 (52.9)	12,262/47,029 (2.14)
EC 3	5,987/60,602 (9.88)	2,180/41,173 (5.29)

[a] Electron micrographs (magnification, × 12,180) were examined with the Global Image Analysis Package, and the data were analyzed by the Wilcoxon rank sum nonparametric test. EC, endothelial cell.

[b] The difference between the areas at 3 and 16 h p.i. was significant ($P = 0.0495$).

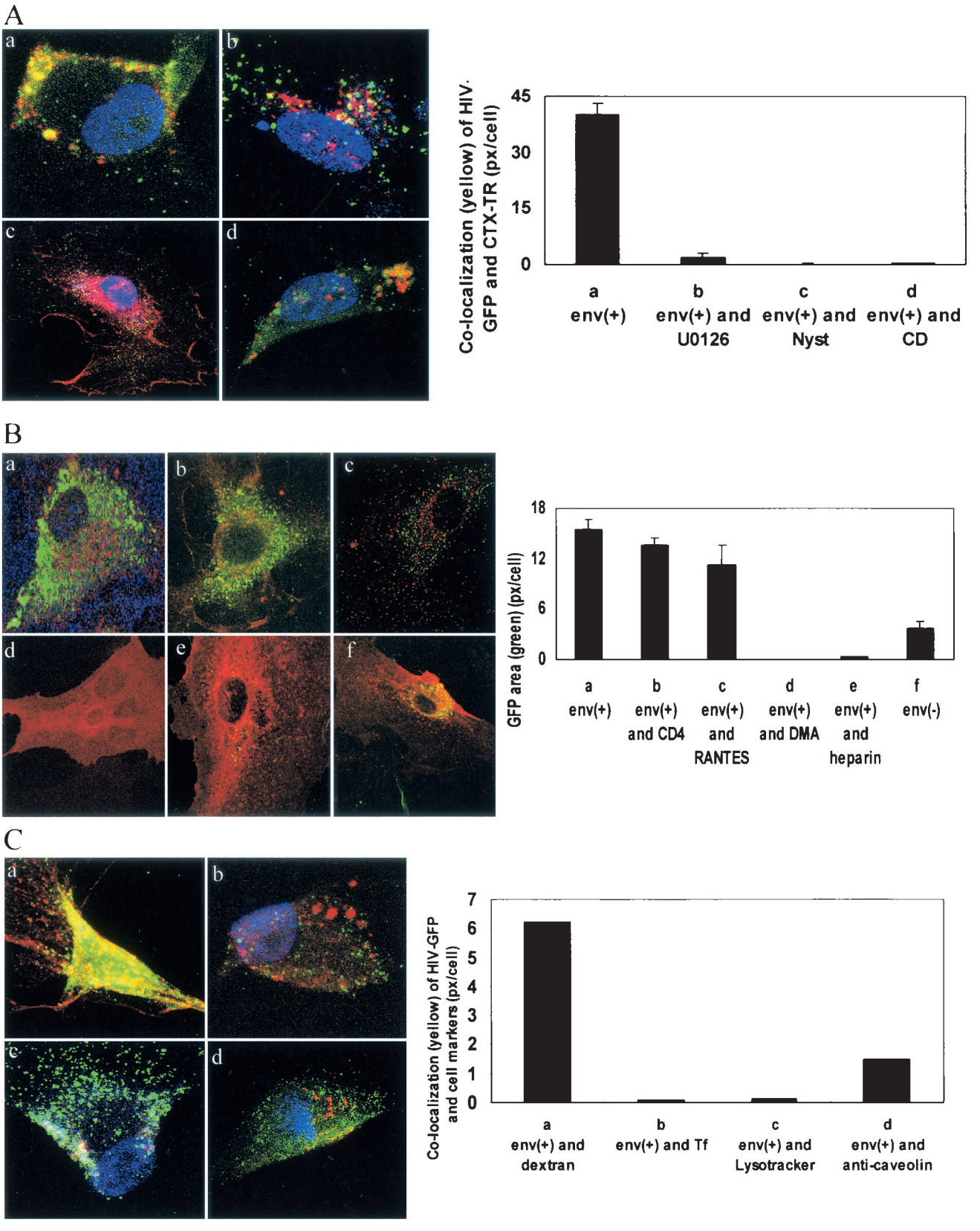

FIG. 8. Virus entry by macropinocytosis. (A) HIV-1 Env$^+$ binds to ganglioside GM1 and enters BMVECs by a process sensitive to inhibition by cholesterol-extracting agents or a MEK inhibitor. BMVECs were not pretreated (a) or were pretreated with U0126 (10 μM for 1 h) (b), nystatin (Nyst) (25 μg/ml for 1 h) (c), or cyclodextrin (CD) (10 mM for 1 h) (d). The cells were then infected with HIV-GFP Env$^+$ (5×10^7 RNA copies); 2.5 h p.i., the cells were stained with cholera toxin B-TR (CTX-TR) (10 μg/ml) for 30 min and fixed, and three cells were then examined by confocal

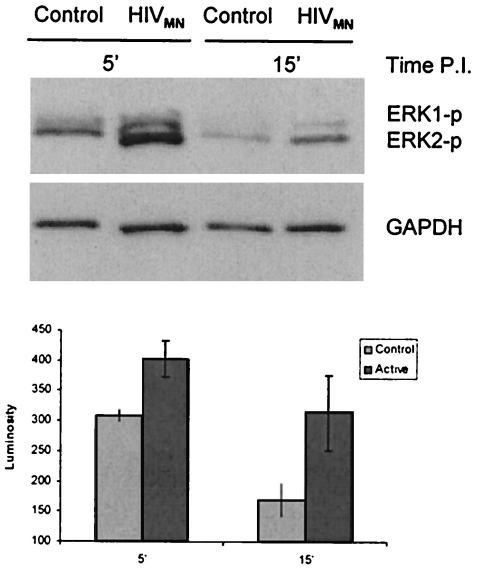

FIG. 9. Virus exposure rapidly activates Erk 1 and 2 in BMVECs. BMVECs were exposed either to vesicles from uninfected cells or to infectious virus (10 μl each) for 5 or 15 min, after which cell lysates were prepared. Erk 1 and 2 activation was determined by Western blotting with antibody against phospho-Erk 1 and 2 (Erk1-p and Erk2-p). The blots were stripped and probed with anti-GAPDH. The error bars indicate standard deviations.

In conclusion, the process of HIV-1 entry into endothelial cells is similar to macropinocytosis recently described with HIV-1 entry into macrophages (31) and can be inhibited by two classes of pharmaceuticals, cholesterol-extracting drugs and heparin. HIV-1 entry is also dependent on Na^+-K^+ transport and MAPK signaling. Virus restructuring of the endothelia with ICAM-1-lined vesicles allows the virus to penetrate the BBB by a transcellular route and allows leukocytes to migrate across the BBB. Thus, both cell-free HIV-1 and HIV-1-infected monocytes/macrophages may gain access to the CNS by the same route.

ACKNOWLEDGMENTS

This work was supported in part by NIH grants DA 10442, HL63065, and HL63639 to M.F., AI42557 and AI50461 to W.P., and HL 48493 to Marlys Witte.

We thank M. Schibler for assistance with confocal microscopic imaging, Q. Zampighi for providing the Zeiss electron microscope, S. Girees and A. Hite for preparing sections for electron microscopy, A. Burns for providing HUVEC, D. Looney for the HIV-1 RNA Amplicor assay, O. Schwartz for the HIV-1_{NL4-3} Env$^-$ plasmid, and D. McCreery, HMRI, for assistance with the image analysis program. The AIDS Research and Reference Reagent Program, NIAID, NIH, provided the listed HIV-1 strains and antibodies.

REFERENCES

1. **An, S. F., M. Groves, B. Giometto, A. A. Beckett, and F. Scaravilli.** 1999. Detection and localisation of HIV-1 DNA and RNA in fixed adult AIDS brain by polymerase chain reaction/in situ hybridisation technique. Acta Neuropathol. (Berlin) **98:**481–487.
2. **An, S. F., M. Groves, F. Gray, and F. Scaravilli.** 1999. Early entry and widespread cellular involvement of HIV-1 DNA in brains of HIV-1 positive asymptomatic individuals. J. Neuropathol. Exp. Neurol. **58:**1156–1162.
3. **Banks, W. A., E. O. Freed, K. M. Wolf, S. M. Robinson, M. Franko, and V. B. Kumar.** 2001. Transport of human immunodeficiency virus type 1 pseudoviruses across the blood-brain barrier: role of envelope proteins and adsorptive endocytosis. J. Virol. **75:**4681–4691.
4. **Berger, E.** 1997. HIV entry and tropism: the chemokine receptor connection. AIDS **11:**S3-S16.
5. **Berger, O., X. Gan, C. Gujuluva, A. R. Burns, G. Sulur, M. Stins, D. Way, M. Witte, M. Weinand, J. Said, K. S. Kim, D. Taub, M. C. Graves, and M. Fiala.** 1999. CXC and CC chemokine receptors on coronary and brain endothelia. Mol. Med. **5:**795–805.
6. **Bernfield, M., M. Gotte, P. W. Park, O. Reizes, M. L. Fitzgerald, J. Lincecum, and M. Zako.** 1999. Functions of cell surface heparan sulfate proteoglycans. Annu. Rev. Biochem. **68:**729–777.
7. **Chan, D. C., and P. S. Kim.** 1998. HIV entry and its inhibition. Cell **93:**681–684.
8. **Chen, Y., and L. C. Norkin.** 1999. Extracellular simian virus 40 transmits a signal that promotes virus enclosure within caveolae. Exp. Cell Res. **246:**83–90.
9. **Dalgleish, A. G., P. C. Beverley, P. R. Clapham, D. H. Crawford, M. F. Greaves, and R. A. Weiss.** 1984. The CD4 (T4) antigen is an essential component of the receptor for the AIDS retrovirus. Nature **312:**763–767.
10. **Deckert-Schluter, M., D. Schluter, H. Hof, O. D. Wiestler, and H. Lassmann.** 1994. Differential expression of ICAM-1, VCAM-1 and their ligands LFA-1, Mac-1, CD43, VLA-4, and MHC class II antigens in murine Toxoplasma encephalitis: a light microscopic and ultrastructural immunohistochemical study. J. Neuropathol. Exp. Neurol. **53:**457–468.
11. **de Vries, H. E., M. C. Blom-Roosemalen, M. van Oosten, A. G. de Boer, T. J. van Berkel, D. D. Breimer, and J. Kuiper.** 1996. The influence of cytokines on the integrity of the blood-brain barrier in vitro. J. Neuroimmunol. **64:**37–43.
12. **Eckert, D. M., and P. S. Kim.** 2001. Mechanisms of viral membrane fusion and its inhibition. Annu. Rev. Biochem. **70:**777–810.
13. **Engelhardt, B., F. K. Conley, and E. C. Butcher.** 1994. Cell adhesion molecules on vessels during inflammation in the mouse central nervous system. J. Neuroimmunol. **51:**199–208.
14. **Etienne-Manneville, S., J. B. Manneville, P. Adamson, B. Wilbourn, J. Greenwood, and P. O. Couraud.** 2000. ICAM-1-coupled cytoskeletal rearrangements and transendothelial lymphocyte migration involve intracellular calcium signaling in brain endothelial cell lines. J. Immunol. **165:**3375–3383.
15. **Fantini, J., M. Maresca, D. Hammache, N. Yahi, and O. Delezay.** 2000. Glycosphingolipid (GSL) microdomains as attachment platforms for host pathogens and their toxins on intestinal epithelial cells: activation of signal transduction pathways and perturbations of intestinal absorption and secretion. Glycoconj. J. **17:**173–179.
16. **Feng, D., J. A. Nagy, J. Hipp, H. F. Dvorak, and A. M. Dvorak.** 1996. Vesiculo-vacuolar organelles and the regulation of venule permeability to macromolecules by vascular permeability factor, histamine, and serotonin. J. Exp. Med. **183:**1981–1986.
17. **Feng, D., J. A. Nagy, K. Pyne, I. Hammel, H. F. Dvorak, and A. M. Dvorak.** 1999. Pathways of macromolecular extravasation across microvascular endo-

microscopy (magnification, ×95). Using an overlay of approximately 30 confocal sections from each examined cell, the area of colocalization (yellow) (pixels/cell) was scanned and is shown on the *y* axis of the graph. (B) HIV-1 Env$^+$ binding and entry is not reduced by anti-CD4, is partially inhibited by AOP-RANTES, and is completely inhibited by heparin or dimethylamiloride. BMVECs either were not pretreated (a and f) or were pretreated for 30 min with anti-CD4 (10 μg/ml) (b), for 1 h with AOP-RANTES (100 nM) (c), or for 1 h with dimethylamiloride (DMA) (20 μM) (d). The cells were then infected with HIV-GFP Env$^+$ (5×10^7 RNA copies) (a to d), HIV-GFP Env$^+$ (5×10^7 RNA copies) preincubated for 5 min with heparin (20 μg/ml) (e), or HIV-GFP Env$^-$ (4.6×10^7 RNA copies) (f). Cholera toxin B-TR was added 2.5 h p.i., the cells were fixed 3 h p.i., three single sections were examined in each cell by confocal microscopy (magnification, ×95), and the area of GFP (green) (pixels/cell) was scanned and is shown on the *y* axis of the graph. (C) HIV-1 Env$^+$ strongly colocalizes with fluid phase marker, weakly with caveolin and Lysotracker, and not at all with transferrin. The cells were infected with GFP–HIV-1 Env$^+$; 2.5 h p.i., the cells were stained with TR-dextran (1 mg/ml) (a), TR-transferrin (20 μg/ml) (b), or Lysotracker dye (75 nM) (c), and anti-caveolin staining (d) was done after fixation. The cells were then examined by confocal microscopy (magnification, ×95); using an overlay of approximately 30 sections from each examined cell, the area of colocalization (yellow) (pixels/cell) was scanned and is shown on the *y* axis of the graph. The error bars indicate standard deviations.

thelium in response to VPF/VEGF and other vasoactive mediators. Microcirculation **6:**23–44.
18. **Fiala, M., D. J. Looney, M. Stins, D. D. Way, L. Zhang, X. Gan, F. Chiappelli, E. S. Schweitzer, P. Shapshak, M. Weinand, M. C. Graves, M. Witte, and K. S. Kim.** 1997. TNF-alpha opens a paracellular route for HIV-1 invasion across the blood-brain barrier. Mol. Med. **3:**553–564.
19. **Furuchi, T., and R. G. Anderson.** 1998. Cholesterol depletion of caveolae causes hyperactivation of extracellular signal-related kinase (ERK). J. Biol. Chem. **273:**21099–21104.
20. **Gendelman, H., L. Baca, C. Kubrak, P. Genis, S. Burrous, R. M. Friedman, D. Jacobs, and M. Meltzer.** 1992. Induction of IFN-alpha in peripheral blood mononuclear cells by HIV-infected monocytes. Restricted antiviral activity of the HIV-induced IFN. J. Immunol. **148:**422–429.
21. **Georgsson, G.** 1994. Neuropathologic aspects of lentiviral infections. Ann. N. Y. Acad. Sci. **724:**50–67.
22. **Gujuluva, C., A. R. Burns, T. Pushkarsky, W. Popik, O. Berger, M. Bukrinsky, M. C. Graves, and M. Fiala.** 2001. HIV-1 penetrates coronary artery endothelial cells by transcytosis. Mol. Med. **7:**169–176.
23. **Hug, P., H. M. Lin, T. Korte, X. Xiao, D. S. Dimitrov, J. M. Wang, A. Puri, and R. Blumenthal.** 2000. Glycosphingolipids promote entry of a broad range of human immunodeficiency virus type 1 isolates into cell lines expressing CD4, CXCR4, and/or CCR5. J. Virol. **74:**6377–6385.
24. **Kozak, S. L., J. M. Heard, and D. Kabat.** 2002. Segregation of CD4 and CXCR4 into distinct lipid microdomains in T lymphocytes suggests a mechanism for membrane destabilization by human immunodeficiency virus. J. Virol. **76:**1802–1815.
25. **Lee, E. S., H. Zhou, and A. J. Henderson.** 2001. Endothelial cells enhance human immunodeficiency virus type 1 replication in macrophages through a C/EBP-dependent mechanism. J. Virol. **75:**9703–9712.
26. **Liu, Y., X. P. Tang, J. C. McArthur, J. Scott, and S. Gartner.** 2000. Analysis of human immunodeficiency virus type 1 gp160 sequences from a patient with HIV dementia: evidence for monocyte trafficking into brain. J. Neurovirol. **6**(Suppl. 1)**:**S70-S81.
27. **Lossinsky, A. S., K. F. Buttle, R. Pluta, M. J. Mossakowski, and H. M. Wisniewski.** 1999. Immunoultrastructural expression of intercellular adhesion molecule-1 in endothelial cell vesiculotubular structures and vesiculovacuolar organelles in blood-brain barrier development and injury. Cell Tissue Res. **295:**77–88.
28. **Manes, S., G. del Real, R. A. Lacalle, P. Lucas, C. Gomez-Mouton, S. Sanchez-Palomino, R. Delgado, J. Alcami, E. Mira, and A. C. Martinez.** 2000. Membrane raft microdomains mediate lateral assemblies required for HIV-1 infection. EMBO Rep. **1:**190–196.
29. **Mankowski, J., J. Spelman, H. Ressetar, J. Strandberg, J. Laterra, D. L. Carter, J. E. Clements, and M. C. Zink.** 1994. Neurovirulent simian immunodeficiency virus replicates productively in endothelial cells of the central nervous system in vivo and in vitro. J. Virol. **68:**8202–8208.
30. **Marechal, V., F. Clavel, J. M. Heard, and O. Schwartz.** 1998. Cytosolic Gag p24 as an index of productive entry of human immunodeficiency virus type 1. J. Virol. **72:**2208–2212.
31. **Marechal, V., M. C. Prevost, C. Petit, E. Perret, J. M. Heard, and O. Schwartz.** 2001. Human immunodeficiency virus type 1 entry into macrophages mediated by macropinocytosis. J. Virol. **75:**11166–11177.
32. **Massari, F. E., G. Poli, S. M. Schnittman, M. C. Psallidopoulos, V. Davey, and A. S. Fauci.** 1990. In vivo T lymphocyte origin of macrophage-tropic strains of HIV. Role of monocytes during in vitro isolation and in vivo infection. J. Immunol. **144:**4628–4632.
33. **McClure, M. O., M. Marsh, and R. A. Weiss.** 1988. Human immunodeficiency virus infection of CD4-bearing cells occurs by a pH-independent mechanism. EMBO J. **7:**513–518.
34. **Moses, A. V., F. E. Bloom, C. D. Pauza, and J. A. Nelson.** 1993. Human immunodeficiency virus infection of human brain capillary endothelial cells occurs via a CD4/galactosylceramide-independent mechanism. Proc. Natl. Acad. Sci. USA **90:**10474–10478.
35. **Nguyen, D. H., and J. E. Hildreth.** 2000. Evidence for budding of human immunodeficiency virus type 1 selectively from glycolipid-enriched membrane lipid rafts. J. Virol. **74:**3264–3272.
36. **Nichols, B. J., A. K. Kenworthy, R. S. Polishchuk, R. Lodge, T. H. Roberts, K. Hirschberg, R. D. Phair, and J. Lippincott-Schwartz.** 2001. Rapid cycling of lipid raft markers between the cell surface and Golgi complex. J. Cell Biol. **153:**529–541.
37. **Pelkmans, L., J. Kartenbeck, and A. Helenius.** 2001. Caveolar endocytosis of simian virus 40 reveals a new two-step vesicular-transport pathway to the ER. Nat. Cell Biol. **3:**473–483.
38. **Planz, O., S. Pleschka, and S. Ludwig.** 2001. MEK-specific inhibitor U0126 blocks spread of Borna disease virus in cultured cells. J. Virol. **75:**4871–4877.
39. **Pleschka, S., T. Wolff, C. Ehrhardt, G. Hobom, O. Planz, U. R. Rapp, and S. Ludwig.** 2001. Influenza virus propagation is impaired by inhibition of the Raf/MEK/ERK signalling cascade. Nat. Cell Biol. **3:**301–305.
40. **Poland, S. D., G. P. Rice, and G. A. Dekaban.** 1995. HIV-1 infection of human brain-derived microvascular endothelial cells in vitro. J. Acquir. Immune Defic. Syndr. Hum. Retrovirol. **8:**437–445.
41. **Popik, W., T. Alce, and W.-C. Au.** 2002. Immunodeficiency virus type 1 uses lipid raft-localized CD4 and chemokine receptors for productive entry into CD4+ T cells. J. Virol. **76:**4709–4722.
42. **Popik, W., J. E. Hesselgesser, and P. M. Pitha.** 1998. Binding of HIV-1 to CD4 and CXCR4 receptors differentially regulates expression of inflammatory genes and activates the MEK/ERK signaling pathway. J. Virol. **72:**6406–6413.
43. **Popik, W., and P. M. Pitha.** 1996. Binding of human immunodeficiency virus type 1 to CD4 induces association of Lck and Raf-1 and activates Raf-1 by a Ras-independent pathway. Mol. Cell. Biol. **16:**6532–6541.
44. **Popik, W., and P. M. Pitha.** 2000. Inhibition of CD3/CD28-mediated activation of the MEK/ERK signaling pathway represses replication of X4 but not R5 human immunodeficiency virus type 1 in peripheral blood CD4(+) T lymphocytes. J. Virol. **74:**2558–2566.
45. **Resnick, L., J. R. Berger, P. Shapshak, and W. W. Tourtellotte.** 1988. Early penetration of the blood-brain-barrier by HIV. Neurology **38:**9–14.
46. **Romero, I. A., M. C. Prevost, E. Perret, P. Adamson, J. Greenwood, P. O. Couraud, and S. Ozden.** 2000. Interactions between brain endothelial cells and human T-cell leukemia virus type 1-infected lymphocytes: mechanisms of viral entry into the central nervous system. J. Virol. **74:**6021–6030.
47. **Rossio, J. L., M. T. Esser, K. Suryanarayana, D. K. Schneider, J. W. Bess, Jr., G. M. Vasquez, T. A. Wiltrout, E. Chertova, M. K. Grimes, Q. Sattentau, L. O. Arthur, L. E. Henderson, and J. D. Lifson.** 1998. Inactivation of human immunodeficiency virus type 1 infectivity with preservation of conformational and functional integrity of virion surface proteins. J. Virol. **72:**7992–8001.
48. **Schaeffer, E., R. Geleziunas, and W. C. Greene.** 2001. Human immunodeficiency virus type 1 Nef functions at the level of virus entry by enhancing cytoplasmic delivery of virions. J. Virol. **75:**2993–3000.
49. **Schmidtmayerova, H., M. Alfano, G. Nuovo, and M. Bukrinsky.** 1998. Human immunodeficiency virus type 1 T-lymphotropic strains enter macrophages via a CD4- and CXCR4-mediated pathway: replication is restricted at a postentry level. J. Virol. **72:**4633–4642.
50. **Simons, K., and E. Ikonen.** 1997. Functional rafts in cell membranes. Nature **387:**569–572.
51. **Stantchev, T. S., and C. C. Broder.** 2001. Human immunodeficiency virus type-1 and chemokines: beyond competition for common cellular receptors. Cytokine Growth Factor Rev. **12:**219–243.
52. **van Nieuw Amerongen, G. P., S. van Delft, M. A. Vermeer, J. G. Collard, and V. W. van Hinsbergh.** 2000. Activation of RhoA by thrombin in endothelial hyperpermeability: role of Rho kinase and protein tyrosine kinases. Circ. Res. **87:**335–340.
53. **Wu, X., H. Liu, H. Xiao, J. Kim, P. Seshaiah, G. Natsoulis, J. D. Boeke, B. H. Hahn, and J. C. Kappes.** 1995. Targeting foreign proteins to human immunodeficiency virus particles via fusion with Vpr and Vpx. J. Virol. **69:**3389–3398.
54. **Zhang, L., D. Looney, D. Taub, S. L. Chang, D. Way, M. H. Witte, M. C. Graves, and M. Fiala.** 1998. Cocaine opens the blood-brain barrier to HIV-1 invasion. J. Neurovirol. **4:**619–626.